ACS APPLIED MATERIALS & INTERFACES

Research Article

www.acsami.org

Photovoltaic Property of a Vertically Aligned Carbon Nanotube Hexagonal Network Assembled with CdS Quantum Dots

Chen Li, Jun Xia, Qilong Wang, Jing Chen,* Chi Li, Wei Lei, and Xiaobing Zhang

School of Electronic Science and Engineering, Southeast University, Nanjing, China, 210096

ABSTRACT: A vertically aligned carbon nanotube (VACNT) hexagonal network was fabricated by plasma enhanced chemical vapor deposition as an electrode scaffold to assemble CdS quantum dots (QDs). The quantum dot sensitized solar cell (QDSSC) based on a VACNT/CdS hexagonal network shows a short circuit current density of 4.7 mA/cm^2, which is almost twice of that based on screen-printed CNT/CdS thin film with the same thickness. The enhancement of the short circuit current could be attributed to the unique morphology of the VACNT hexagonal network, which provides direct and percolating pathways for the electrons to transfer, enhances the spectral transmission through the hexagonal microchannels to the photoactive QD sites, and also presents more surface area to assembled CdS QDs without consuming extra substrate space. The photovoltaic property of the VACNT/CdS hexagonal network indicates its potential application in the energy conversion devices.

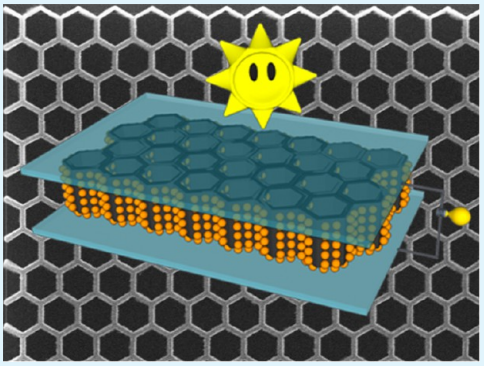

KEYWORDS: *quantum dot, solar cell, CdS, carbon nanotubes, photovoltaics, short circuit current*

INTRODUCTION

The emergence of semiconductor quantum dots (QDs) as light harvesters has stimulated extensive interests for their applications of photovoltaic devices.[1−3] Due to the size-dependent band gap of the QDs like CdS,[4,5] CdSe.[6,7] and PbS,[8,9] it offers the possibility to readily tune the optical absorption throughout the UV and near-infrared spectral regions by selecting the particle size. QDs are especially appealing also for their high extinction coefficients compared with the conventional dye molecules.[10,11] In addition, the utilization of multiple exciton generation of QDs is expected to further enhance the performance of QD based photovoltaic devices.[12]

Recent works reported that high-performance dye-sensitized solar cells (DSSCs) with electrodes of TiO_2 and InP nanostructures attain power conversion efficiencies which were exceeded by 11 and 13%, respectively.[13,14] However, the organic solar cells or quantum dot sensitized solar cells (QDSSCs) which utilize random oriented carbon nanotubes (CNTs) as their electrodes normally have efficiencies below 1%.[15−19] One of the factors which affect the efficiency is the limited short circuit current which relies on the ability of the photoactive materials to efficiently absorb photons, dissociate excitons, and transport charge carriers to the respective electrodes.[20,21] However, these processes could be hampered by the disordered electron transport path[22] and the recombination of electron−hole pairs.[23,24] The vertically aligned nanostructures, such as carbon nanotubes (CNTs), TiO_2 nanotubes, and ZnO nanowires, which were employed as direct electron pathways, have been proved to provide an effective charge transport.[25−27] A previous study reveals that the single wall carbon nanotubes (SWCNTs) were employed as a network to disperse TiO_2 particles. An increase of photoconversion efficiency indicates the beneficial role of the SWCNTs as conducting scaffolds to collect and transport charges.[17] Low growth temperature (~500 °C) facilitated with a plasma enhanced chemical vapor deposition (PECVD) system makes vertically aligned CNTs (VACNTs) more attractive than randomly oriented CNTs for photovoltaic applications, not only because the VACNTs can be used as direct conducting pathways to capture and transport electrons from the QDs to the electrode surface along the nanotubes but also because they enhance the light transmission of the electrode when the light irradiates perpendicularly to the substrate.[26,28]

In this work, we fabricated the VACNT hexagonal network as electrode scaffolds in a QDSSC photoanode to anchor CdS QDs. By the combination of exciton generation in CdS QDs and the direct electron transport characteristics of VACNTs, we have succeeded in demonstrating a VACNT/CdS based QDSSC and its photovoltaic properties were also investigated.

EXPERIMENTAL SECTION

Fluorine-doped tin dioxide (FTO)/quartz (Solaronix) substrates (10 mm × 10 mm) were first ultrasonically cleaned by deionized (DI) water, acetone, and isopropyl alcohol consecutively and then dried at 100 °C in an oven. The VACNT hexagonal network fabrication details are described in our previous work elsewhere.[29] The VACNTs were grown in a PECVD system (AIXTRON-Black Magic) at 500 °C with a

Received: May 8, 2013
Accepted: July 11, 2013
Published: July 11, 2013

   dx.doi.org/10.1021/am401725x | ACS Appl. Mater. Interfaces 2013, 5, 7400−7404

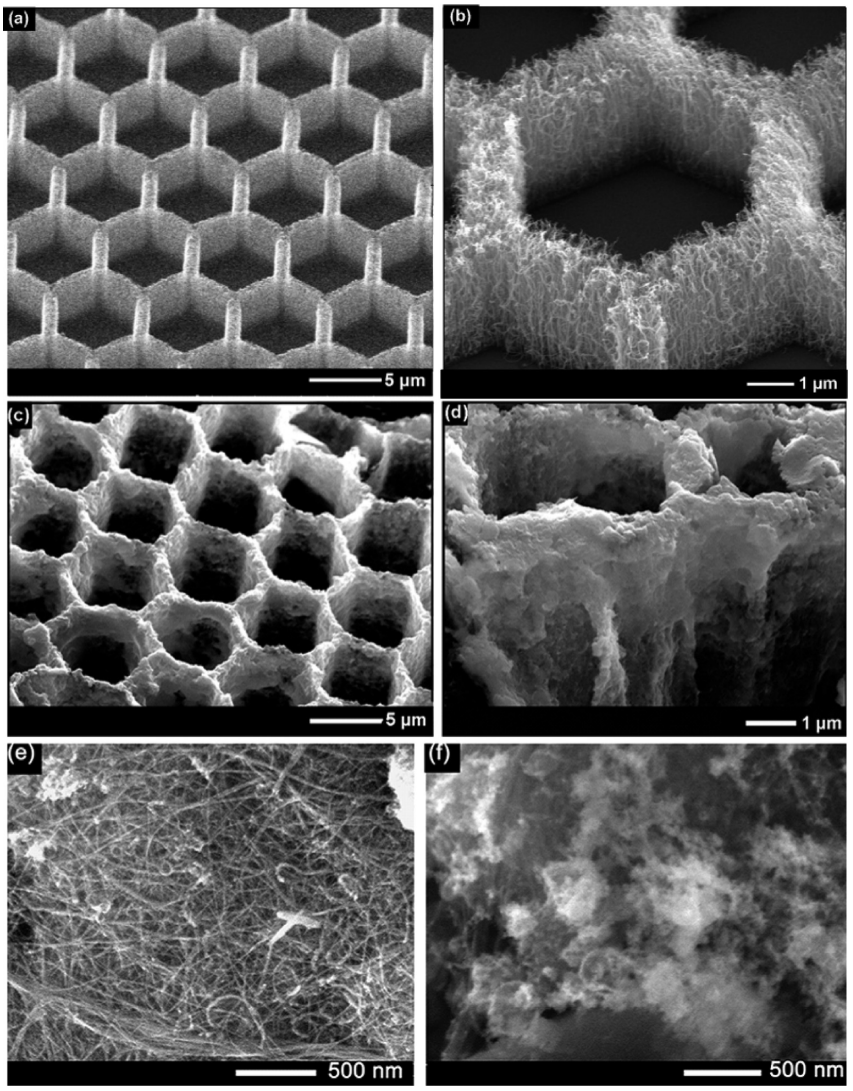

Figure 1. (a) Low and (b) high magnification SEM images of the VACNT hexagonal network. (c) Low and (d) high magnification SEM images of the VACNT hexagonal network after 5 min of electrodepositing with CdS QDs. (e) SEM image of the screen-printed CNTs. (f) SEM image of the screen-printed CNTs after 5 min of electrodepositing with CdS QDs.

7 nm thick layer of Ni catalyst. Photolithography and lift-off processes were utilized to pattern the catalyst layer with periodical hexagonal rings with 6 μm spacing. Then, substrate with VACNTs was immersed in an ethanol solution containing 0.5 M $Cd(NO_3)_2$ for 5 min. Electrodeposition was performed by applying a potential of 1.0 V vs SCE (saturated calomel electrode) at room temperature in the 0.1 M Na_2S methanol solution with time varying from 2 to 8 min. After that, the photoanode composed of VACNT/CdS was prepared. Meanwhile, another photoanode made of CNT thin film by the screen-printed process was also prepared for comparison.[30] CdS QDs deposited on the screen-printed CNT thin film were processed with the same method mentioned above. A Pt layer was evaporated on a piece of ITO glass substrate which served as the counter electrode. Finally, the photoanode was placed in parallel with the counter electrode, and the internal space of these two electrodes was filled with liquid electrolyte solution of polysulfide consisting of 2 M Na_2S and 3 M S. Herein, QDSSCs with a photoanode consisting of screen-printed CNT/CdS thin film (8 min of electrodeposition) and a VACNT/CdS hexagonal network (5 min of electrodeposition) are defined as cells A and B, respectively.

Solar Cell Characterization. The measurements of photovoltage and photocurrent response under on−off cycle were performed using an electrochemical workstation (CHI-660D) with a 150 W xenon arc lamp (Oriel). The active cell area was typically 0.25 cm^2. The current density−voltage (J−V) characteristics were measured with a sourcemeter (Keithley 2440), and the cell was subjected to the irradiation of a solar simulator (Abet-technologies, USA) operating at 100 mW/cm^2 (AM 1.5G). The incident photon-to-current conversion efficiency (IPCE) was measured with a QE/IPCE Measurement Kit (Oriel, USA) in the wavelength range 300−600 nm. The absorption spectra were recorded by a UV−visible spectrometer (SHIMADZU MPC-2200).

RESULTS AND DISCUSSION

Parts a and b of Figure 1 illustrate the scanning electron micrograph (SEM) images of the VACNT hexagonal network with low and high magnification, respectively. It can be seen that the honeycomb-shaped network consists of uniform interconnected hexagonal microchannels with 6 μm spacing. The VACNTs grow perpendicularly to the substrate in well-defined order with a height of 5 μm. Such a three-dimensional hexagonal network offers more surface area to anchor the QDs without consuming extra substrate space. It is expected to serve as an electrode scaffold to capture and transport the photogenerated electrons. After the electrodeposition process, the surface of the film turns from black to dark yellow and then

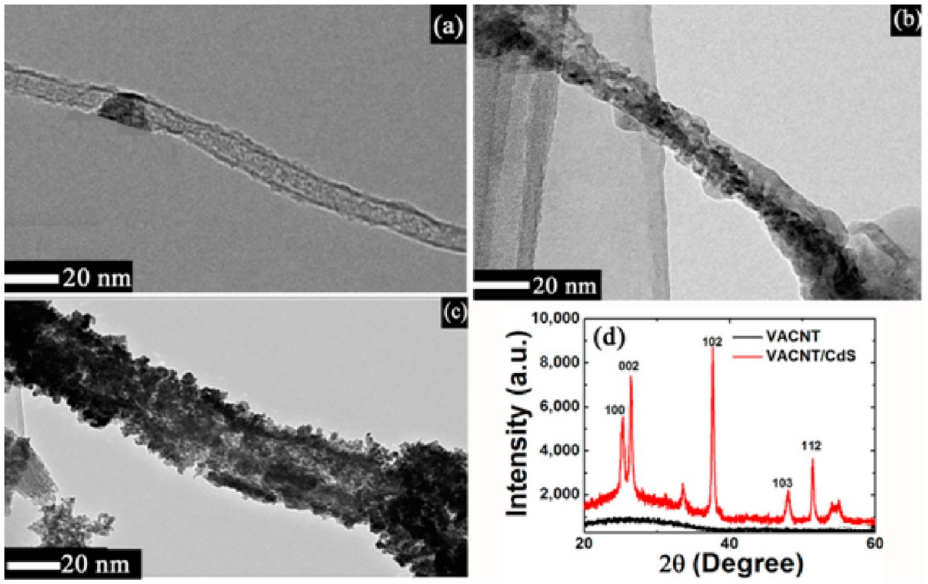

Figure 2. (a) TEM images of one single CNT from the VACNT hexagonal network. One single CNT electrodeposited with CdS QDs after (b) 2 min and (c) 5 min, respectively. (d) XRD spectra of pure VACNT and after 5 min of electrodepositing with CdS QDs.

to orange, indicating that CdS nanoparticles have been deposited on the VACNTs. Each nanotube can span the entire photoanode thickness which leads to a built-in percolation pathway for an efficient transport of electrons. Parts c and d of Figure 1 represent the SEM images of the VACNT hexagonal network after 5 min of electrodepositing with CdS QDs in low and high magnification, respectively. The sidewalls and grids of the network are densely covered by CdS QDs. The SEM images of screen-printed CNTs before and after 5 min of electrodepositing with CdS QDs are shown in Figure 1e and f, respectively. CNTs are randomly oriented and entangled together to form a thin film with 5 μm thickness which is the same height as the VACNT hexagonal network. Therefore, CdS QDs are mainly deposited on the top surface of the CNT film. It is worth noting that, due to the presence of a Schottky barrier at the nanotube–metal junction, it is possible for VACNTs (work function Φ = 5.0 eV) to achieve an ohmic contact to a metal with a similar work function such as Ni (Φ = 5.1 eV), which we used as a catalyst.[31,32] Thus, a photovoltaic device employing the VACNT hexagonal network which is directly grown on the substrate could possibly have an improved photoresponse current.

Figure 2a illustrates the transmission electron microscopy (TEM) image of one single CNT with a diameter of ~10 nm from the VACNT hexagonal network. After 2 min (Figure 2b) and 5 min (Figure 2c) of electrodepositing, the CdS nanoparticles with a size of less than 10 nm are uniformly and densely dispersed on the surface of VACNTs. Figure 2d shows the X-ray diffraction spectra (XRD) of the VACNT hexagonal network and after 5 min of electrodepositing with CdS QDs. There is no obvious peak shown in the XRD spectra of the pure VACNT photoanode. The VACNT/CdS diffraction peaks at 25.2, 26.3, 38.6, 48.1, and 51.4° are indexed to the wurtzite structure of CdS (JCPDS no. 01-0783).

Figure 3a shows the energy dispersive X-ray (EDX) spectroscopy of the VACNT/CdS hexagonal network. The sharp peaks represent the sample is mainly composed of C, Cd, and S elements contained in CNTs and CdS nanostructures. Figure 3b shows the absorption spectra for photoanodes based

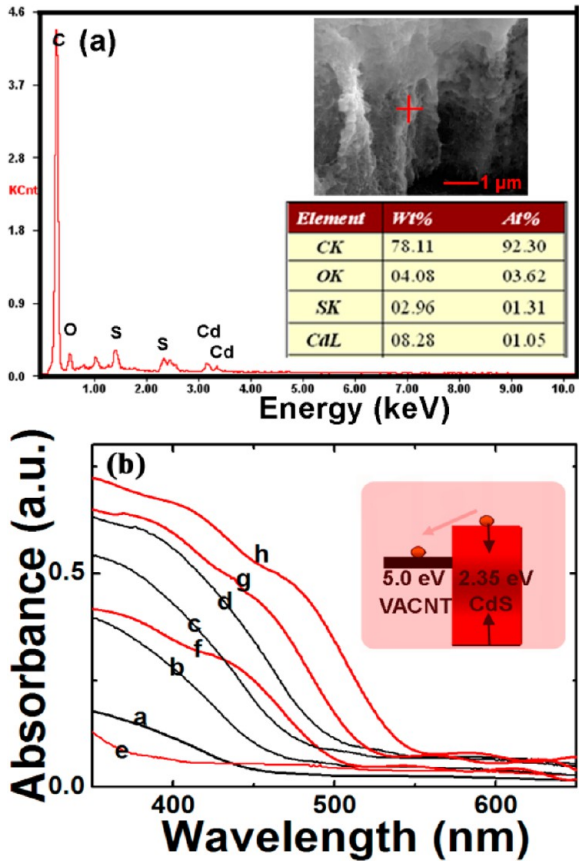

Figure 3. (a) EDX spectra of VACNTs after 5 min of electrodepositing with CdS QDs. (b) Absorption spectra of photoanodes of pure screen-printed CNTs, VACNTs, and after electrodepositing CdS QDs on them with different times. Curve a, pure screen-printed CNTs; curve b, CNT/CdS (2 min); curve c, CNT/CdS (5 min); curve d, CNT/CdS (8 min); curve e, pure VACNTs; curve f, VACNT/CdS (2 min); curve g, VACNT/CdS (5 min); curve h, VACNT/CdS (8 min). The inset is the energy band diagram of VACNT and CdS.

dx.doi.org/10.1021/am401725x | ACS Appl. Mater. Interfaces 2013, 5, 7400–7404

on screen-printed CNTs and the VACNT hexagonal network with different electrodepositing times varying from 2 to 8 min. The pure CNTs and VACNTs almost have no absorption in the visible region. After electrodepositing with CdS QDs on them, the absorption spectra become broader and more intensive as the electrodepositing time increased. The VACNT/CdS (5 min) (curve g) has an extended coverage of spectra range compared with the CNT/CdS (8 min) (curve d), which indicates that more CdS QDs were assembled on VACNTs. The absorption edges, obtained from the intersection of the sharply decreasing region of a spectrum with its baseline, are ~530 nm for VACNT/CdS (5 min), corresponding to a band gap of approximately 2.35 eV. The energy band diagram of CNT and CdS is shown in the inset of Figure 3b. Therefore, it can be observed that the conduction bands of the CdS and the work function of CNT form an energy step for the electron transport.

The key characteristic for a solar cell is the power conversion efficiency (PCE), which is defined as

$$\eta = (I_M \times V_M)/P_{in} = (FF \times I_{sc} \times V_{oc})/P_{in}$$

I_M and V_M describe the bias point at which the power generation reaches the maximum, and I_{sc} and V_{oc} are the short circuit current and open circuit voltage. P_{in} is the incident power density. Parts a and b of Figure 4 illustrate the

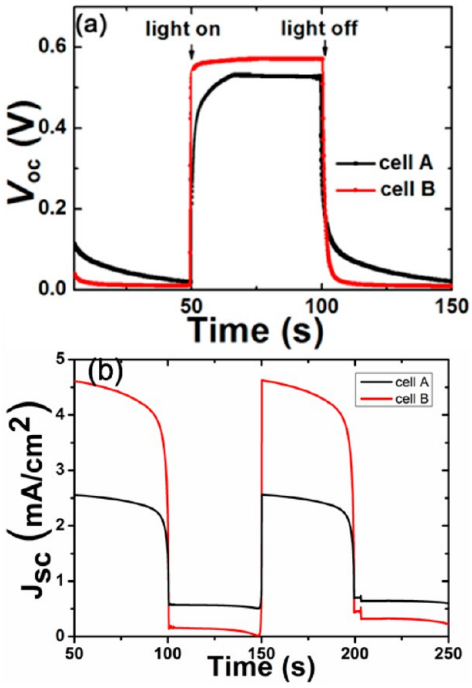

Figure 4. (a) Photovoltage and (b) photocurrent density responses of cell A (screen-printed CNT/CdS based QDSSC with 8 min of electrodepositing) and cell B (VACNT/CdS hexagonal network based QDSSC with 5 min of electrodepositing) versus time profiles.

photovoltage and photocurrent response to repeated on–off cycles of visible irradiation, respectively. The V_{oc} value of cell B (VACNT/CdS hexagonal network based QDSSC with 5 min of electrodepositing) is 0.58 V, which is 0.05 V higher and more stable than that of cell A (screen-printed CNT/CdS based QDSSC with 8 min of electrodepositing). For the short current density (J_{sc}) of cell B, it drops to zero when the light is turned off, and quickly recovers to the highest value of 4.6 mA/cm^2, which is almost 1.8 times the value of cell A (2.6 mA/cm^2). It is suspected that the low loss characteristic enhanced by the effective linearity of the VACNT scaffolds gives more spectral transmission through the hexagonal microchannel directly to the photoactive QD sites. In addition, the possible ohmic contact of as-grown VACNTs with the substrate gives a lower resistivity which could attribute to an enhanced photocurrent.

Figure 5a shows the compared photocurrent–voltage (J–V) characteristics for cells A and B. Cell A exhibits V_{oc} = 0.53 V, J_{sc}

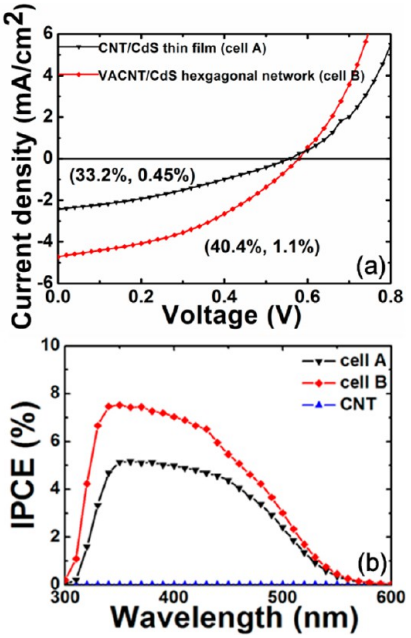

Figure 5. (a) Current density–voltage characteristics and (b) IPCE spectra for cell A and cell B. Cell A exhibits V_{oc} = 0.53 V, J_{sc} = 2.4 mA/cm^2, FF = 33.2%, and efficiency = 0.45%, whereas cell B shows V_{oc} = 0.58 V, J_{sc} = 4.7 mA/cm^2, FF = 40.4%, and efficiency = 1.1%.

= 2.4 mA/cm^2, FF = 33.2%, and efficiency = 0.45%, whereas cell B shows V_{oc} = 0.58 V, J_{sc} = 4.7 mA/cm^2, FF = 40.4%, and efficiency = 1.1%. By comparing with cell A, the performance of cell B is improved by 2.4 times in efficiency. The increase in J_{sc}, which consequently improves the PCE, can be attributed to three benefits of the VACNT/CdS hexagonal network: (i) The presence of direct and percolation conduction pathways for electrons, which eventually prevents charge recombination. The 5 μm long VACNTs grow perpendicularly to the substrate; then, a thick active layer with efficient charge transport capability could be realized. (ii) The channels in each hexagonal unit allow more spectral transmission to the photoactive QD sites when the light irradiates perpendicularly to the substrate. (iii) The enhanced surface area of the electrode increases the number of assembled QDs.

As shown in Figure 5b, we evaluated the QDSSC performance of cell A, cell B, and pure CNTs by recording the incident photon-to-current conversion efficiency (IPCE) in the range 300–600 nm. The IPCE was calculated by

$$\text{IPCE}\ (\%) = 1240 J_{sc}/\lambda I_{inc} \times 100$$

where I_{inc} is the power of the incident light.[33] Clearly, the IPCE value for the pure CNT is very small; it almost has no photoresponse. The IPCE values for cells A and B at 350 nm are 5 and 7.5%, respectively. The increase of photoconversion

dx.doi.org/10.1021/am401725x | ACS Appl. Mater. Interfaces 2013, 5, 7400–7404

efficiency is an indication of the improved charge collection and transport by introducing the VACNT hexagonal network as an electrode scaffold in the photoanode.

CONCLUSIONS

In conclusion, we report the fabrication of VACNT/CdS hexagonal network based QDSSC which exhibits an enhanced short circuit current compared with that of the screen-printed CNT/CdS based QDSSC. The short circuit current was almost doubled, while the PCE reached 1.1%. These results were achieved by combining the properties of exciton generation in CdS QDs and the distinct electron transport property of VACNTs. So far, the efficiency remained low compared with that of high-performance DSSCs, but the successful incorporation of the QDs with the VACNT hexagonal network into solar cells has been demonstrated. It is possible that further efficiency enhancement could be realized by utilizing the VACNT hexagonal network in DSSCs.

AUTHOR INFORMATION

Corresponding Author

*E-mail: chenjingmoon@gmail.com. Phone: +86 25 83792449. Fax: +86 25 833632222.

Notes

The authors declare no competing financial interest.

ACKNOWLEDGMENTS

This work was supported partially by the National Key Basic Research Program 973 (2013CB328803, 2010CB327705), the National High-Tech R&D Program 863 of China (2012AA03A302, 2013AA011004) National Natural Science Foundation Project (51002031, 61007036, 61101023, 51202028, and 51120125001), Foundation of Doctoral Program of Ministry of Education under Grant (20100092120022, 20120092120025), and the Chinese 111 Project (B07027).

REFERENCES

(1) Nazeeruddin, M. K.; Pechy, P.; Renouard, T.; Zakeeruddin, S. M.; Humphry-Baker, R.; Comte, P.; Liska, P.; Cevey, L.; Costa, E.; Shklover, V.; Spiccia, L.; Deacon, G. B.; Bignozzi, C. A.; Gratzel, M. *J. Am. Chem. Soc.* **2001**, *123*, 1613−1624.
(2) Barve, A. V.; Krishna, S. *Appl. Phys. Lett.* **2012**, *100*, 191107.
(3) Mar, J. D.; Xu, X. L.; Baumberg, J. J.; Irvine, A. C.; Stanley, C.; Williams, D. A. *J. Appl. Phys.* **2011**, *110*, 053110.
(4) Yu, K. H.; Lu, G. H.; Chen, K. H.; Mao, S.; Kim, H.; Chen, J. H. *Nanoscale* **2012**, *4*, 742−746.
(5) Luo, J. H.; Wei, H. Y.; Huang, Q. L.; Hu, X.; Zhao, H. F.; Yu, R. C.; Li, D. M.; Luo, Y. H.; Meng, Q. B. *Chem. Commun.* **2013**, *49*, 3881−3883.
(6) Chen, J.; Song, J. L.; Sun, X. W.; Deng, W. Q.; Jiang, C. Y.; Lei, W.; Huang, J. H.; Liu, R. S. *Appl. Phys. Lett.* **2009**, *94*, 3.
(7) Tian, J. J.; Zhang, Q. F.; Zhang, L. L.; Gao, R.; Shen, L. F.; Zhang, S. G.; Qu, X. H.; Cao, G. Z. *Nanoscale* **2013**, *5*, 936−943.
(8) Chang, L. Y.; Lunt, R. R.; Brown, P. R.; Bulovic, V.; Bawendi, M. G. *Nano Lett.* **2013**, *13*, 994−999.
(9) Kim, G. H.; Kim, H. B.; Walker, B.; Choi, H.; Yang, C.; Park, J.; Kim, J. Y. *ACS Appl. Mater. Interfaces* **2013**, *5*, 1757−1760.
(10) Choi, H.; Nicolaescu, R.; Paek, S.; Ko, J.; Kamat, P. V. *ACS Nano* **2011**, *5*, 9238−9245.
(11) Kavan, L.; Yum, J. H.; Nazeeruddin, M. K.; Gratzel, M. *ACS Nano* **2011**, *5*, 9171−9178.
(12) Nozik, A. J. *Inorg. Chem.* **2005**, *44*, 6893−6899.
(13) Gao, F.; Wang, Y.; Shi, D.; Zhang, J.; Wang, M. K.; Jing, X. Y.; Humphry-Baker, R.; Wang, P.; Zakeeruddin, S. M.; Gratzel, M. *J. Am. Chem. Soc.* **2008**, *130*, 10720−10728.
(14) Wallentin, J.; Anttu, N.; Asoli, D.; Huffman, M.; Aberg, I.; Magnusson, M. H.; Siefer, G.; Fuss-Kailuweit, P.; Dimroth, F.; Witzigmann, B.; Xu, H. Q.; Samuelson, L.; Deppert, K.; Borgstrom, M. T. *Science* **2013**, *339*, 1057−60.
(15) Miller, A. J.; Hatton, R. A.; Chen, G. Y.; Silva, S. R. P. *Appl. Phys. Lett.* **2007**, 90.
(16) Miller, A. J.; Hatton, R. A.; Silva, S. R. P. *Appl. Phys. Lett.* **2006**, 89.
(17) Kongkanand, A.; Dominguez, R. M.; Kamat, P. V. *Nano Lett.* **2007**, *7*, 676−680.
(18) Dutta, M.; Basak, D. *J. Nanopart. Res.* **2011**, *13*, 5311−5319.
(19) Paul, G. S.; Kim, J. H.; Kim, M. S.; Do, K.; Ko, J.; Yu, J. S. *ACS Appl. Mater. Interfaces* **2012**, *4*, 375−381.
(20) Hodes, G. *J. Phys. Chem. C* **2008**, *112*, 17778−17787.
(21) Kamat, P. V. *J. Phys. Chem. C* **2008**, *112*, 18737−18753.
(22) Borchert, H.; Witt, F.; Chanaewa, A.; Werner, F.; Dorn, J.; Dufaux, T.; Kruszynska, M.; Jandke, A.; Holtig, M.; Alfere, T.; Bottcher, J.; Gimmler, C.; Klinke, C.; Burghard, M.; Mews, A.; Weller, H.; Parisi, J. *J. Phys. Chem. C* **2012**, *116*, 412−419.
(23) Yang, H. B.; Guo, C. X.; Guai, G. H.; Song, Q. L.; Jiang, S. P.; Li, C. M. *ACS Appl. Mater. Interfaces* **2011**, *3*, 1940−1945.
(24) Sheeney-Haj-Khia, L.; Basnar, B.; Willner, I. *Angew. Chem., Int. Ed.* **2005**, *44*, 78−83.
(25) Hao, F.; Dong, P.; Zhang, J.; Zhang, Y. C.; Loya, P. E.; Hauge, R. H.; Li, J. B.; Lou, J.; Lin, H. *Sci. Rep.* **2012**, *2*, 368.
(26) Gao, X. F.; Li, H. B.; Sun, W. T.; Chen, Q.; Tang, F. Q.; Peng, L. M. *J. Phys. Chem. C* **2009**, *113*, 7531−7535.
(27) Chen, J.; Li, C.; Eda, G.; Zhang, Y.; Lei, W.; Chhowalla, M.; Milnecf, W. I.; Deng, W. Q. *Chem. Commun.* **2011**, *47*, 6084−6086.
(28) Farrow, B.; Kamat, P. V. *J. Am. Chem. Soc.* **2009**, *131*, 11124.
(29) Li, C.; Zhang, Y.; Mann, M.; Hiralal, P.; Unalan, H. E.; Lei, W.; Wang, B.; Chu, D.; Pribat, D.; Amaratunga, G. A. J.; Milne, W. I. *Appl. Phys. Lett.* **2010**, *96*, 143114.
(30) Yoshihara, K.; Fujii, S.; Kawai, H.; Ishida, K.; Honda, S. I.; Katayama, M. *Appl. Phys. Lett.* **2007**, *91*, 113109.
(31) Min, Y. S.; Bae, E. J.; Kim, U. J.; Park, W.; Hwang, C. S. *Appl. Phys. Lett.* **2007**, *90*, 263104.
(32) Javey, A.; Guo, J.; Wang, Q.; Lundstrom, M.; Dai, H. *Nature* **2003**, *424*, 654−657.
(33) Gratzel, M. *Inorg. Chem.* **2005**, *44*, 6841−6851.